Output-Redefinition-Based Dynamic Inversion Control for a Nonminimum Phase Hypersonic Vehicle

Linqi Ye, Qun Zong, *Member, IEEE*, John L. Crassidis, and Bailing Tian, *Member, IEEE*

***Abstract*—Output-redefinition-based dynamic inversion (ORDI) control is proposed for a nonminimum phase hypersonic vehicle (HSV). When velocity and altitude are selected as control outputs, an HSV exhibits nonminimum phase behavior, preventing the application of standard dynamic inversion control due to the unstable zero dynamics. This problem is solved by the ORDI control architecture, where output redefinition is utilized at first to render the modified zero dynamics stable, and then, dynamic inversion is used to stabilize the new external dynamics. Three kinds of ORDI controllers with different choices of new control output are investigated. The first takes the internal variable as the control output, which exhibits good robustness but with restricted performance. The second utilizes a synthetic output, which is a linear combination of the system output and internal variable, making the zero dynamics adjustable, and thus improves the tracking performance. The third adds an integral item to the synthetic output, and thus ensures zero steady-state error even with model uncertainties. A systematic way is proposed to determine the combination coefficient to achieve zero dynamics assignment by using the root locus method. The efficiency of the method is illustrated by numerical simulations.**

***Index Terms*—Dynamic inversion, hypersonic vehicle (HSV), nonminimum phase, output redefinition, zero dynamics assignment.**

I. Introduction

HYPERSONIC vehicles (HSVs) refer to vehicles that travels at velocity greater than Mach 5. This is regarded as one of the most promising technology for achieving cost effective and reliable access to space. One of the most difficult challenges encountered in designing flight control systems for HSVs is the nonminimum phase problem due to elevator-to-lift coupling [1]. When the nonlinear control method, dynamic inversion, is straightforwardly applied to nonminimum phase systems, it results in exact tracking but the unstable zero dynamics remains an unstable part in the closed-loop system. Therefore, the nonminimum phase character of an HSV prevents the application of standard dynamic inversion and all of its invariants, bringing great challenges to nonlinear controller design for these vehicles.

The nonminimum phase problem of HSV can be avoided by adding a canard. Since the elevator-to-lift coupling is canceled by the canard, the nonminimum phase behavior is removed. Many nonlinear methods are applied to the canard configured HSV, such as sliding mode control [2]–[4], dynamic surface control [5]–[7], and feedback linearization control [8], [9], to name a few. Although a canard is beneficial to avoid the nonminimum phase problem, it is a problem for the vehicle structure since the canard must withstand a large thermal stress at hypersonic speeds. Therefore, it is of great significance to investigate the control problem of an HSV without a canard, which means that a controller must be designed directly based on the nonminimum phase HSV model. This issue has received more and more attention in recent years but only a few new control methods have been proposed [1], [10]–[15].

Though the nonminimum phase character of an HSV limits the application of classical nonlinear control methods, linear control methods are still available. In [10], a linear controller is developed for an HSV by the pole assignment method. As an improvement, a stable inversion approach [16], [17] was applied to an HSV in [11]. It achieves exact tracking by imbedding the ideal internal dynamics into a linear feedback controller. However, this method is noncausal and greatly depends on exact model knowledge.

In addition, some nonlinear control methods are proposed for a nonminimum phase HSV. One typical method is approximate feedback linearization [12], [13]. By strategically ignoring the elevator-to-lift coupling and resorting to dynamic extension at the input side, an approximate model with full vector relative degree is obtained. Then, standard dynamic inversion can be applied to the approximate model, resulting in approximate linearization of the original model. Other methods can also be used to the approximate model, such as backstepping [14]. This method works mainly because the approximate model has higher relative degree so that the internal variables are included in the

Manuscript received February 27, 2017; revised June 11, 2017 and August 10, 2017; accepted September 7, 2017. Date of publication October 6, 2017; date of current version January 5, 2018. This work was supported in part by the National Natural Science Foundation of China under Grant 61673294, Grant 61503323, and Grant 61773278; in part by the China Scholarship Council under Grant 201606250160; and in part by the Ministry of Education Equipment Development Fund under Grant 6141A02033311. *(Corresponding author: Bailing Tian.)*

L. Ye, Q. Zong, and B. Tian are with the School of Electrical and Information Engineering, Tianjin University, Tianjin 300072, China (e-mail: yelinqi@tju.edu.cn; zongqun@tju.edu.cn; bailing_tian@tju.edu.cn).

J. L. Crassidis is with the Department of Mechanical and Aerospace Engineering, University at Buffalo, The State University of New York, Amherst, NY 14260-4400 USA (e-mail: johnc@buffalo.edu).

Color versions of one or more of the figures in this paper are available online at http://ieeexplore.ieee.org.

Digital Object Identifier 10.1109/TIE.2017.2760246

control loop. However, this method only works when the coupling is weak enough, i.e., a "slightly" nonminimum phase system [18]. The control law designed by the approximate model will result in instability when applied to the model with stronger nonminimum phase behavior [13].

Another nonlinear control method focuses on the redefinition of the zero dynamics. In [1], a preliminary feedback transformation is used to convert the model into the interconnection of systems with feedforward and feedback form, respectively. Then, the original output is converted into a state trajectory of new zero dynamics. Hence, additional control effort is not required for stabilizing the internal dynamics. In [15], with the definition of two separate nested zero dynamics subsystems, the elevator is treated as the primary effector to control the regulated output and the stabilization of the internal dynamics as a secondary objective.

The idea of the two aforementioned papers is very similar to the output redefinition method [19], whose main concept is: first, to perform an output redefinition such that the zero dynamics with respect to the new output are acceptable; and second, to define a modified desired trajectory for the new output to track such that the original output tracks the original desired trajectory asymptotically. Since the second step can be realized by stable inversion [16], [17], the main difficulty lies in how to find a minimum phase output. In [19], the new output is constructed through the B-I norm form. But it is nontrivial to implement in practice since the B-I norm form of a complex system is usually difficult to obtain. In [20], the flatness-based approach is proposed, where a variable with full relative degree is selected as the control output. This variable is called by the flat output, and there is no zero dynamics corresponding to it. However, no systemic way is provided to find such a flat output, which limits the application of this method. Another method is statically equivalent output [21], [22], where the new output is computed on the basis of the solution of a singular partial differential equation to induce the prescribed zero dynamics.

Inspired by [1] and [19], an output-redefinition-based dynamic inversion (ORDI) control method is developed to achieve stable tracking control for a nonminimum phase HSV. The ORDI method combines the advantage of linear and nonlinear control. In the first step, the zero dynamics are stabilized by constructing a synthetic output, which is a linear combination of the system output, an internal variable and integral tracking error, whose effect is very similar to Proportional-Integral (PI) control. In the second step, the external dynamics are stabilized by dynamic inversion, which takes advantage of nonlinear control. As a result, the closed-loop system becomes an asymptotic stable linear system cascaded with a locally stable nonlinear zero dynamics. Based on the ORDI control architecture, three kinds of ORDI controllers are developed for the HSV with different choices of the new output definitions.

The main contributions of this paper are twofold. First, for the nonminimum phase system control theory, a systematic way is proposed to construct a minimum phase output. By selecting the new output as a linear combination of the system output, an internal variable and integral tracking error, and using the root locus method to determine the combination coefficient, an effective way is proposed to achieve zero dynamics assignment. Compared to the methods in the aforementioned references [19]–[22], the proposed method is based on the original coordinate and the classical root locus method, making it much easier to be carried out, especially for complex systems. Second, for the HSV control problem, the ORDI method is successfully applied to solve the nonminimum phase problem. The proposed method has advantages over the existing ones [1], [10]–[15]. Compared to the linear methods [10], [11], the developed method is nonlinear, which takes advantage of dynamic inversion control. Compared to [12]–[14], this method is able to deal with stronger nonminimum phase behavior due to the inclusion of the zero dynamics assignment process. Finally, compared to [1] and [15], this method transfers the high-order control problem into two control problems of lower order, which greatly simplifies the control design.

Fig. 1. X-43A.

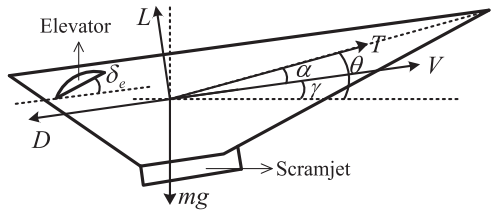

Fig. 2. Axes of the HSV.

The remainder of this paper is organized as follows. In Section II, the HSV model and its zero dynamics analysis are presented. The main idea of ORDI control is provided in Section III. Then, the ORDI controllers for an HSV will be developed in Sections IV and V. Next, simulations and discussions are given in Section VI. Finally, the conclusions are summarized in Section VII.

II. HSV Model and Zero Dynamics Analysis

A. Nonminimum Phase HSV Model

The model considered in this paper is the rigid-body longitudinal model of an air-breathing HSV, which is developed in [1] to verify the control algorithm for HSV with nonminimum phase characteristics. The model is based on NASA's scramjet-powered X-43A, as shown in Figs. 1 and 2.

The model comprises five state variables $\mathbf{x} = [V, h, \gamma, \theta, Q]^T$, representing velocity, altitude, flight path angle, pitch angle, and pitch rate, respectively. There are two control inputs $\mathbf{u} = [\phi, \delta_e]^T$, representing fuel to air ratio into the scramjet combustor and the elevator deflection angle, respectively. The control inputs indirectly affect the dynamics of the aircraft through the forces and moments: T, D, L, and M.

TABLE I
VEHICLE PARAMETERS

Notation	Meaning	Value
m	Vehicle mass	147.9 slug/ft
g	Acceleration due to gravity	32.17 ft/s^2
I_{yy}	Moment of inertia	86 722.5 slug·ft^2/rad
S	Reference area	17 ft^2
$\bar{c}$	Mean aerodynamic chord	17 ft
z_T	Thrust-to-moment coupling coefficient	8.36 ft
ρ_0	Air density at nominal altitude	6.7429×10^{-5} slugs/ft^3
h_s	Inverse of the air density exponential decay rate	21 358.8 ft
h_0	Nominal altitude	85 000 ft

Following [1], the dynamic equations of the model are written as

$$\begin{cases} \dot{V} = (T\cos\alpha - D - mg\sin\gamma)/m \\ \dot{h} = V\sin\gamma \\ \dot{\gamma} = (L + T\sin\alpha - mg\cos\gamma)/(mV) \\ \dot{\theta} = Q \\ \dot{Q} = M/I_{yy}. \end{cases} \tag{1}$$

The expressions for thrust T, lift L, drag D, and the pitching moment M are given by

$$\begin{aligned} T &= \bar{q}S\left[C_T(\alpha) + C_{T\phi}(\alpha)\phi\right] \\ L &= \bar{q}S\left[C_L(\alpha) + C_L^{\delta_e}\delta_e\right] \\ D &= \bar{q}SC_D(\alpha) \\ M &= z_T T + \bar{q}\bar{c}S\left[C_M(\alpha) + C_M^{\delta_e}\delta_e\right] \end{aligned} \tag{2}$$

where

$$\begin{aligned} C_T(\alpha) &= C_T^3\alpha^3 + C_T^2\alpha^2 + C_T^1\alpha + C_T^0 \\ C_{T\phi}(\alpha) &= C_T^{\phi\alpha^3}\alpha^3 + C_T^{\phi\alpha^2}\alpha^2 + C_T^{\phi\alpha}\alpha + C_T^{\phi} \\ C_L(\alpha) &= C_L^{\alpha}\alpha + C_L^0 \\ C_D(\alpha) &= C_D^{\alpha^2}\alpha^2 + C_D^{\alpha}\alpha + C_D^0 \\ C_M(\alpha) &= C_M^{\alpha^2}\alpha^2 + C_M^{\alpha}\alpha + C_M^0. \end{aligned} \tag{3}$$

The angle of attack α satisfies $\alpha = \theta - \gamma$. The dynamic pressure $\bar{q}$ is calculated by $\bar{q} = \rho(h)V^2/2$ with $\rho(h) = \rho_0 \mathrm{e}^{-(h-h_0)/h_s}$ being the atmospheric density. All the parameter values in the model are shown in Tables I and II [1], [23].

The system outputs are $[V, h]^T$ and the admissible flight range is $\Xi_y := \{7500 \le V \le 11\,000(\mathrm{ft/s}), 70\,000 \le h \le 135\,000(\mathrm{ft})\}$. The control objective is to design a control law $\mathbf{u} = [\phi, \delta_e]^T$ such that the system outputs track the given constant commands V^*, h^* asymptotically in the admissible flight range Ξ_y.

B. Zero Dynamics Analysis for Standard Dynamic Inversion

In standard dynamic inversion, the system outputs $[V, h]^T$ are employed as control outputs. According to [24], zero dynamics are the remaining dynamics when the outputs are identically zero. Denote the tracking errors as $e_V = V - V^*, e_h = h - h^*$.

TABLE II
AERODYNAMIC PARAMETERS

Notation	Value	Notation	Value	Notation	Value
C_L^{α}	5.9598 rad^{-1}	$C_M^{\alpha^2}$	6.8888 ft^{-1}	$C_T^{\phi\alpha}$	0.69341 rad^{-1}
$C_L^{\delta_e}$	0.73408 rad^{-1}	C_M^{α}	5.1390 ft^{-1}	C_T^{ϕ}	0.19904
C_L^0	−0.024377	C_M^0	0.16277	C_T^3	1.0929 rad^{-3}
$C_D^{\alpha^2}$	7.9641 rad^{-2}	$C_M^{\delta_e}$	−1.3642 rad^{-1}	C_T^2	0.97141 rad^{-1}
C_D^{α}	−0.074020 rad^{-1}	$C_T^{\phi\alpha^3}$	−14.038 rad^{-3}	C_T^1	0.037275 rad^{-1}
C_D^0	−0.019880 rad^{-2}	$C_T^{\phi\alpha^2}$	−1.5839 rad^{-1}	C_T^0	−0.021635

Since the commands V^*, h^* are nonzero, the tracking errors $[e_V, e_h]^T$ will be used as regulated outputs to analyze the zero dynamics.

For the convenience of zero dynamics analysis and control design, the HSV model (4) is rewritten in an affine form as

$$\begin{cases} \dot{V} = f_V + g_V\phi \\ \dot{h} = V\sin\gamma \\ \dot{\gamma} = f_\gamma + g_{\gamma\phi}\phi + g_{\gamma\delta}\delta_e \\ \dot{\theta} = Q \\ \dot{Q} = f_q + g_{q\phi}\phi + g_{q\delta}\delta_e \end{cases} \tag{4}$$

where

$$\begin{aligned} f_V &= (\bar{q}SC_T(\alpha)\cos\alpha - \bar{q}SC_D(\alpha) - mg\sin\gamma)/m \\ g_V &= \bar{q}SC_{T\phi}(\alpha)\cos\alpha/m \\ f_\gamma &= (\bar{q}SC_L(\alpha) + \bar{q}SC_T(\alpha)\sin\alpha - mg\cos\gamma)/(mV) \\ g_{\gamma\phi} &= \bar{q}SC_{T\phi}(\alpha)\sin\alpha/(mV),\ g_{\gamma\delta} = \bar{q}SC_L^{\delta_e}/(mV) \\ f_q &= (z_T\bar{q}SC_T(\alpha) + \bar{q}\bar{c}SC_M(\alpha))/I_{yy} \\ g_{q\phi} &= z_T\bar{q}SC_{T\phi}(\alpha)/I_{yy},\ g_{q\delta} = \bar{q}\bar{c}SC_M^{\delta_e}/I_{yy}. \end{aligned} \tag{5}$$

With the regulated outputs $\mathbf{y} = [e_V, e_h]^T$, the external dynamics are

$$\begin{bmatrix} \dot{e}_V \\ \ddot{e}_h \end{bmatrix} = \begin{bmatrix} f_V \\ f_h \end{bmatrix} + \begin{bmatrix} g_V & 0 \\ g_{h\phi} & g_{h\delta} \end{bmatrix} \begin{bmatrix} \phi \\ \delta_e \end{bmatrix} \tag{6}$$

where

$$\begin{aligned} f_h &= f_V\sin\gamma + f_\gamma V\cos\gamma \\ g_{h\phi} &= g_V\sin\gamma + g_{\gamma\phi}V\cos\gamma \\ g_{h\delta} &= g_{\gamma\delta}V\cos\gamma. \end{aligned} \tag{7}$$

When the regulated outputs are identically zero, the inputs can be derived by setting the right side of (6) to zero, which are

$$\begin{bmatrix} \phi^0 \\ \delta_e^0 \end{bmatrix} = \begin{bmatrix} g_V & 0 \\ g_{h\phi} & g_{h\delta} \end{bmatrix}^{-1} \begin{bmatrix} -f_V \\ -f_h \end{bmatrix}. \tag{8}$$

Substituting (8) into the θ, Q dynamics yields

$$\begin{aligned} \dot{\theta} &= Q \\ \dot{Q} &= f_q + g_{q\phi}\phi^0 + g_{q\delta}\delta_e^0. \end{aligned} \tag{9}$$

This is the zero dynamics corresponding to the regulated outputs $\mathbf{y} = [e_V, e_h]^T$, which represents the remaining dynamics

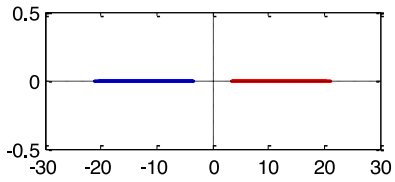

Fig. 3. Root map of the linearized zero dynamics for $\mathbf{y}$.

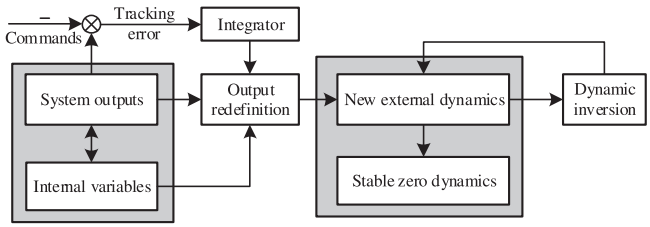

Fig. 4. Schematic diagram of ORDI.

when $e_V \equiv 0,\ e_h \equiv 0$. It can be observed that the zero dynamics is a second-order nonlinear dynamic equation associated with V^*, h^*. The stability can be analyzed by Jacobian linearization. Each time a pair of constant commands V^*, h^* are selected from the range Ξ_y, the zero dynamics are linearized and the roots are calculated. When the whole range Ξ_y is covered, the root map of the linearized zero dynamics is obtained, as shown in Fig. 3. It can be observed that the linearized zero dynamics have a positive real root, indicating that the zero dynamics are unstable with respect to $\mathbf{y} = [e_V, e_h]^T$.

Using standard dynamic inversion means obtaining the control law $[\phi, \delta_e]^T$ by inversion of the external dynamics (6). As a result, when the goal of exact tracking is achieved, i.e.,$e_V = 0,\ e_h = 0$, the remaining dynamics θ, Q become equivalent to the zero dynamics (9), which are unstable. Therefore, standard dynamic inversion is not applicable.

III. Main Concept of ORDI

In order to avoid confusion, it is necessary to state the difference between system outputs and control outputs. In this paper, system outputs refer to the system states that are actually desired to follow some predefined reference commands, whereas control outputs refer to the variables used as outputs for the purpose of controller design. For HSV problems, velocity and altitude are system outputs, and are used as control outputs in standard dynamic inversion. Pitch angle and pitch rate, which cannot be expressed as the combination of the system outputs and their derivatives, are internal variables.

The control scheme of ORDI includes two steps, as shown in Fig. 4.

A. Step 1: Zero Dynamics Assignment by Output Redefinition

By constructing a new control output, the zero dynamics can be modified to make the modified zero dynamics stable. Meanwhile, a proper command should be designed for the new control output to track such that the system output can track the predefined reference trajectory asymptotically, which will be called the equal convergence principle.

Three ways are provided here to construct a minimum phase new output.

1) Internal variable as new output: This way just simply selects the internal variable as a new output, thus it only works for certain systems whose internal variable leads to stable zero dynamics. For an HSV, the internal variable θ can replace the system output V or h as the output. With θ being an output, the corresponding command θ^* is determined by the equilibrium manifold [21] to satisfy the equal convergence principle. Denote $e_\theta = \theta - \theta^*$. Fortunately, it is found that when $\mathbf{y_a} = [e_V, e_\theta]^T$ are chosen as the control outputs, the modified zero dynamics are stable. However, in this way the zero dynamics are fixed and will restrict the tracking performance of the altitude.

2) Static synthetic output: To make the zero dynamics adjustable, the control output can be selected as a linear combination of the system output and the internal variable. In this way, more flexibility is available to improve the tracking performance of the replaced output. For an HSV, the new output is chosen as $\mathbf{y_b} = [e_V, e_h + \lambda_b e_\theta]^T$, where λ_b is a parameter to be designed.

A systematic way is proposed to determine the combination coefficient. First, the root locus of the linearized zero dynamics at one equilibrium is obtained when the coefficient changes. A guiding range of the coefficient is derived such that the root locates in the left-hand plane (LHP). Then, by fixing the coefficient at one possible value in the guiding range, the root map of the linearized zero dynamics at all equilibriums is obtained. Finally, the feasible values for the coefficient with stable zero dynamics can be determined from the root map.

3) Synthetic output with integral: When there are model uncertainties, the command θ^* calculated from the nominal model will no longer satisfy the equal convergence principle. Then, the replaced output, i.e., the altitude, will have steady-state tracking error for the two methods above. This problem can be solved by adding an integral item of the tracking error to the synthetic output, and then zero steady-state error can be guaranteed in the case of model uncertainties for the replaced output. In this case, the new output is chosen as $\mathbf{y_c} = [e_V, e_h + \lambda_{c1} e_\theta + \lambda_{c2}\sigma_h]^T$, where $\dot{\sigma}_h = e_h$ and $\lambda_{c1}, \lambda_{c2}$ are parameters to be designed. Compared to $\mathbf{y_b}$, the additional integral item in $\mathbf{y_c}$ can help to eliminate the altitude tracking error in steady state when there are model uncertainties. The effect is very similar to PI control.

B. Step 2: Dynamic Inversion Control for the New External Dynamics

When the new output is determined, the new external dynamics can be obtained by taking derivatives of the new output until the input appears. Then, dynamic inversion control can be utilized to stabilize the new external dynamics.

After these two steps, the new external dynamics is fully linearized, whereas the whole system is partially linearized. As a result, the closed-loop system becomes a cascade system

$$\begin{aligned} \dot{\mathbf{e}}_\xi &= \mathbf{A}\mathbf{e}_\xi \\ \dot{\mathbf{e}}_\eta &= \mathbf{q}(\mathbf{e}_\xi, \mathbf{e}_\eta) \end{aligned} \tag{10}$$

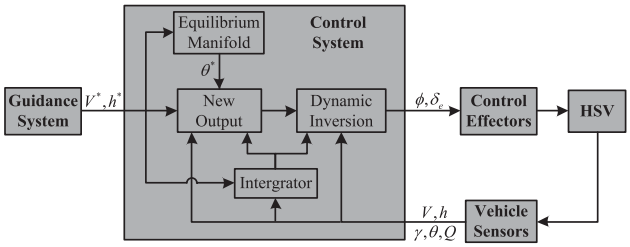

Fig. 5. Block diagram of an HSV flight system.

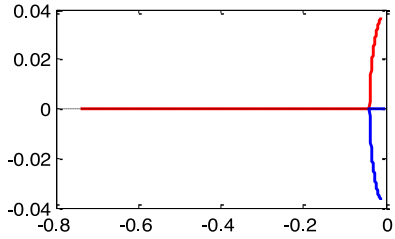

Fig. 6. Root map of linearized zero dynamics for $\mathbf{y_a}$.

where the external dynamics $\mathbf{e}_\xi$ is an independent asymptotic stable linear system, and the internal dynamics $\mathbf{e}_\eta$ is a locally stable nonlinear system influenced by the external states. The Jacobian linearization of (10) is

$$\begin{bmatrix} \dot{\mathbf{e}}_\xi \\ \dot{\mathbf{e}}_\eta \end{bmatrix} = \begin{bmatrix} \mathbf{A} & \mathbf{0} \\ \mathbf{B} & \mathbf{C} \end{bmatrix} \begin{bmatrix} \mathbf{e}_\xi \\ \mathbf{e}_\eta \end{bmatrix} \tag{11}$$

where $\mathbf{B} = \partial \mathbf{q}/\partial \mathbf{e}_\xi$ and $\mathbf{C} = \partial \mathbf{q}/\partial \mathbf{e}_\eta$. The linearized zero dynamics is $\dot{\mathbf{e}}_\eta = \mathbf{C}\mathbf{e}_\eta$. The stability of (11) is determined by a block lower triangular matrix. Since $\mathbf{A}$ and $\mathbf{C}$ are both stabilized in the two steps of ORDI, system (11) is stable.

By applying the ORDI method to an HSV control system, the overall flight system is shown in Fig. 5. In the next two sections, the ORDI controller will be designed for an HSV with different choices of new output.

Remark 1: The new output, which serves as a medium to yield a stable controller, may have no practical meaning. However, since the controller obtained by output redefinition is a state feedback controller, it is available as long as all the system states can be measured. As shown in Fig. 5, when the reference commands of altitude and velocity are given, the corresponding pitch angle command will be calculated and then the new output will be constructed. Then, the control inputs will be calculated by taking dynamic inversion on the new output.

IV. ORDI With Internal Variable as Output

In this section, the pitch angle θ is used to replace the altitude h as an output. In order to satisfy the equal convergence principle, the command θ^* should be chosen as an equilibrium corresponding to V^*, h^*, i.e., θ^* is decided by the equilibrium manifold [21]. For HSV model (1), assume the equilibrium is $\mathbf{x}^* = [V^*, h^*, 0, \theta^*, 0]^T$, with $\mathbf{u}^* = [\phi^*, \delta_e^*]^T$. From $\dot{V} = 0$, $\dot{\gamma} = 0$, and $\dot{Q} = 0$, the following equations can be constructed:

$$\begin{aligned} &\bar{q}^* S \left[C_{T\phi}\left(\theta^*\right)\phi^* + C_T\left(\theta^*\right)\right]\cos\theta^* - \bar{q}^* S C_D\left(\theta^*\right) = 0 \\ &\bar{q}^* S \left[C_L\left(\theta^*\right) + C_L^{\delta_e}\delta_e^*\right] + \bar{q}^* S \left[C_{T\phi}\left(\theta^*\right)\phi^* + C_T\left(\theta^*\right)\right]\sin\theta^* \\ &\quad - mg = 0 \\ &z_T \bar{q}^* S \left[C_{T\phi}\left(\theta^*\right)\phi^* + C_T\left(\theta^*\right)\right] + \bar{q}^* \bar{c} S \left[C_M\left(\theta^*\right) + C_M^{\delta_e}\delta_e^*\right] = 0. \end{aligned} \tag{12}$$

where $\bar{q}^* = \rho_0 e^{-(h^*-h_0)/h_s}(V^*)^2/2$ is the dynamic pressure corresponding to V^*, h^*. In (12), there are three equations with four unknowns $q^*, \theta^*, \phi^*, \delta_e^*$. Once V^*, h^* are given, then $\bar{q}^*$ is determined, and θ^* can be solved from (12). For convenience, denote the solution as follows:

$$\theta^* = q_\theta\left(\bar{q}^*\right). \tag{13}$$

This is the equilibrium manifold [21]. Therefore, the command θ^* for the new output θ can be calculated from (13) according to the given commands V^*, h^*.

A. Zero Dynamics Analysis

With the regulated outputs $\mathbf{y_a} = [e_V, e_\theta]^T$, the external dynamics are as follows:

$$\begin{bmatrix} \dot{e}_V \\ \ddot{e}_\theta \end{bmatrix} = \begin{bmatrix} f_V \\ f_q \end{bmatrix} + \begin{bmatrix} g_V & 0 \\ g_{q\phi} & g_{q\delta} \end{bmatrix} \begin{bmatrix} \phi \\ \delta_e \end{bmatrix}. \tag{14}$$

When the regulated outputs are identically zero, the inputs can be derived by setting the right side of (14) to zero, which are as follows:

$$\begin{bmatrix} \phi^a \\ \delta_e^a \end{bmatrix} = \begin{bmatrix} g_V & 0 \\ g_{q\phi} & g_{q\delta} \end{bmatrix}^{-1} \begin{bmatrix} -f_V \\ -f_q \end{bmatrix}. \tag{15}$$

Substituting (15) into the h, γ dynamics, the zero dynamics are obtained as follows:

$$\begin{aligned} \dot{e}_h &= V\sin\gamma \\ \dot{\gamma} &= f_\gamma + g_{\gamma\phi}\phi^a + g_{\gamma\delta}\delta_e^a. \end{aligned} \tag{16}$$

Fig. 6 shows the root map of the linearized zero dynamics for all V^*, h^* in the range Ξ_y, from which it can be seen that all the roots stay in the LHP. So, $\mathbf{y_a}$ is a minimum phase output and can be used for ORDI control. When the new outputs $\mathbf{y_a} = [e_V, e_\theta]^T$ are driven to zero, the altitude tracking error is determined by the modified zero dynamics (16) and will also converge to zero. However, in this case the modified zero dynamics cannot be adjusted; thus, the altitude tracking performance is restricted.

Remark 2: Root map is employed here to analyze the stability of the zero dynamics around the equilibrium point. However, it is not a global property and only guarantees stability when the system is close to the equilibrium point. For further investigation, a phase portrait of the zero dynamics (16) for the commands $V^* = 8000$ ft/s and $h^* = 100\,000$ ft in the region of interest $\{70\,000 \le h \le 135\,000(\text{ft}), -5 \le \gamma \le 5(\text{deg})\}$ is shown in Fig. 7. It can be observed that any initial value in this region will be attracted to the desired equilibrium point. Similar results can be obtained for other commands.

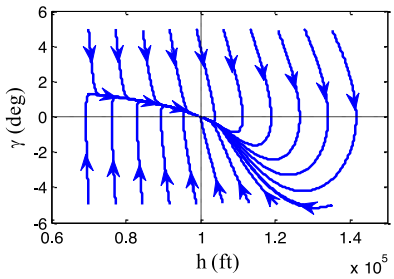

Fig. 7. Phase portrait of the zero dynamics for $\mathbf{y_a}$.

B. Controller Design

According to the new external dynamics (14), design the control inputs as follows:

$$\begin{bmatrix} \phi \\ \delta_e \end{bmatrix} = \begin{bmatrix} g_V & 0 \\ g_{q\phi} & g_{q\delta} \end{bmatrix}^{-1} \begin{bmatrix} -k_{a11}e_V - k_{a12}\sigma_V - f_V \\ -k_{a21}\dot{e}_\theta - k_{a22}e_\theta - k_{a23}\sigma_\theta - f_q \end{bmatrix} \tag{17}$$

where $k_{a11}, k_{a12}, k_{a21}, k_{a22}$, and k_{a23} are positive gains to be designed, and σ_V, σ_θ are integral of the new outputs to cancel model uncertainties

$$\begin{aligned} \dot{\sigma}_V &= e_V \\ \dot{\sigma}_\theta &= e_\theta. \end{aligned} \tag{18}$$

Then, the closed-loop system becomes

$$\begin{bmatrix} \dot{e}_V \\ \ddot{e}_\theta \end{bmatrix} = \begin{bmatrix} -k_{a11}e_V - k_{a12}\sigma_V \\ -k_{a21}\dot{e}_\theta - k_{a22}e_\theta - k_{a23}\sigma_\theta \end{bmatrix}. \tag{19}$$

Finally, the velocity tracking error e_V is determined by the linear equation (19), which can be adjusted almost arbitrarily. However, the altitude tracking error e_h is determined by the modified zero dynamics (16), which is fixed and will restrict the altitude tracking performance.

V. ORDI With Synthetic Output

In this section, a synthetic output is constructed as a linear combination of the system states. First, a static synthetic output is investigated, and then synthetic output with an integral item is investigated.

A. Static Synthetic Output

1) Zero Dynamics Assignment: The new output is chosen as $\mathbf{y_b} = [e_V, e_h + \lambda_b e_\theta]^T$, where λ_b is a parameter to be designed. The adjustable parameter in the new output gives the opportunity to adjust the modified zero dynamics. Denote $e_b = e_h + \lambda_b e_\theta$. The new external dynamics corresponding to the new output are as follows:

$$\begin{bmatrix} \dot{e}_V \\ \ddot{e}_b \end{bmatrix} = \begin{bmatrix} f_V \\ f_b \end{bmatrix} + \begin{bmatrix} g_V & 0 \\ g_{b\phi} & g_{b\delta} \end{bmatrix} \begin{bmatrix} \phi \\ \delta_e \end{bmatrix} \tag{20}$$

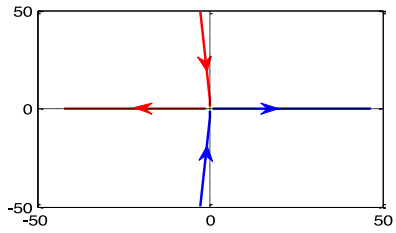

Fig. 8. Root locus of linearized zero dynamics for $\mathbf{y_b}$.

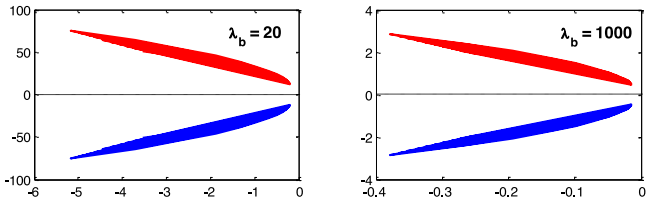

Fig. 9. Root map of linearized zero dynamics for $\mathbf{y_b}$.

where

$$\begin{aligned} f_b &= f_V \sin\gamma + f_\gamma V \cos\gamma + \lambda_b f_q \\ g_{b\phi} &= g_V \sin\gamma + g_{\gamma\phi} V \cos\gamma + \lambda_b g_{q\phi} \\ g_{b\delta} &= g_{\gamma\delta} V \cos\gamma + \lambda_b g_{q\delta}. \end{aligned} \tag{21}$$

The inputs to keep zero outputs are as follows:

$$\begin{bmatrix} \phi^b \\ \delta_e^b \end{bmatrix} = \begin{bmatrix} g_V & 0 \\ g_{b\phi} & g_{b\delta} \end{bmatrix}^{-1} \begin{bmatrix} -f_V \\ -f_b \end{bmatrix}. \tag{22}$$

By substituting (22) into the h, γ dynamics, the modified zero dynamics are as follows:

$$\begin{aligned} \dot{e}_h &= V \sin\gamma \\ \dot{\gamma} &= f_\gamma + g_{\gamma\phi}\phi^b + g_{\gamma\delta}\delta_e^b. \end{aligned} \tag{23}$$

The combination coefficient λ_b will affect the zero dynamics (23) through ϕ^b, δ_e^b since λ_b appears in $f_b, g_{b\phi}, g_{b\delta}$ [see (21)] and then affects ϕ^b, δ_e^b [see (22)]. Therefore, the value of λ_b will have a direct influence on the stability of the modified zero dynamics. A root locus approach will be applied to determine the feasible value of λ_b, which renders stable zero dynamics.

Fig. 8 shows the root locus of the linearized zero dynamics at the equilibrium $\mathbf{x}^* = [8000{,}100\ 000, 0, 0.0231, 0]^T$ when λ_b ranges from -1000 to 1000. The roots are divided into two parts: when $-1000 \le \lambda_b \le 18$, there are two real roots (one positive, one negative), which go away from the origin as λ_b increases; and when $19 \le \lambda_b \le 1000$, there are two LHP complex roots, which go close to the origin as λ_b increases. So, the guiding range is $\lambda_b \ge 19$.

Fig. 9 shows the root map of the linearized zero dynamics for all V^*, h^* in the range Ξ_y with $\lambda_b = 20$ and $\lambda_b = 1000$, respectively. It can be seen that all the roots stay in the LHP. So, $\mathbf{y_b}$ is a minimum phase output for these two values of λ_b, and can be used for ORDI control. The performance for these two values will be compared in the simulations.

When the new outputs $\mathbf{y_b} = [e_V, e_b]^T$ are driven to zero, the altitude tracking error e_h is determined by the modified

zero dynamics (23) and will also converge to zero. However, if there are model uncertainties, the command θ^* calculated from the nominal model no longer satisfies the equal convergence principle; thus, e_h will have steady-state error.

2) Controller Design: According to the new external dynamics (20), design the control inputs as follows:

$$\begin{bmatrix}\phi\\ \delta_e\end{bmatrix}=\begin{bmatrix}g_V & 0\\ g_{b\phi} & g_{b\delta}\end{bmatrix}^{-1}\begin{bmatrix}-k_{b11}e_V-k_{b12}\sigma_V-f_V\\ -k_{b21}\dot{e}_b-k_{b22}e_b-k_{b23}\sigma_b-f_b\end{bmatrix} \tag{24}$$

where $\dot{\sigma}_b=e_b$, and $k_{b11},k_{b12},k_{b21},k_{b22},k_{b23}$ are positive gains to be designed. Then, the closed-loop system becomes

$$\begin{bmatrix}\dot{e}_V\\ \ddot{e}_b\end{bmatrix}=\begin{bmatrix}-k_{b11}e_V-k_{b12}\sigma_V\\ -k_{b21}\dot{e}_b-k_{b22}e_b-k_{b23}\sigma_b\end{bmatrix}. \tag{25}$$

Finally, the velocity tracking error decided by (25) can achieve a prescribed tracking performance, whereas the altitude tracking error, decided by the modified zero dynamics (23), can also be adjusted to some extent by tuning λ_b.

B. Synthetic Output With Integral

1) Zero Dynamics Assignment: On the basis of the synthetic output $\mathbf{y_b}=[e_V,e_h+\lambda_b e_\theta]^T$, an integral item can be added to deal with model uncertainties. So, the new output is chosen as $\mathbf{y_c}=[e_V,e_h+\lambda_{c1}e_\theta+\lambda_{c2}\sigma_h]^T$, where $\lambda_{c1},\lambda_{c2}$ are parameters to be designed. Denote $e_c=e_h+\lambda_{c1}e_\theta+\lambda_{c2}\sigma_h$. The new external dynamics corresponding to the new output are as follows:

$$\begin{bmatrix}\dot{e}_V\\ \ddot{e}_c\end{bmatrix}=\begin{bmatrix}f_V\\ f_c\end{bmatrix}+\begin{bmatrix}g_V & 0\\ g_{c\phi} & g_{c\delta}\end{bmatrix}\begin{bmatrix}\phi\\ \delta_e\end{bmatrix} \tag{26}$$

where

$$\begin{aligned}f_c&=f_V\sin\gamma+f_\gamma V\cos\gamma+\lambda_{c1}f_q+\lambda_{c2}V\sin\gamma\\ g_{c\phi}&=g_V\sin\gamma+g_{\gamma\phi}V\cos\gamma+\lambda_{c1}g_{q\phi}\\ g_{c\delta}&=g_{\gamma\delta}V\cos\gamma+\lambda_{c1}g_{q\delta}.\end{aligned} \tag{27}$$

The inputs to keep zero outputs are as follows:

$$\begin{bmatrix}\phi^c\\ \delta_e^c\end{bmatrix}=\begin{bmatrix}g_V & 0\\ g_{c\phi} & g_{c\delta}\end{bmatrix}^{-1}\begin{bmatrix}-f_V\\ -f_c\end{bmatrix}. \tag{28}$$

Due to the introduction of the integral item, σ_h becomes an additional internal variable. Substituting (28) into the σ_h,h,γ dynamics, the modified zero dynamics are as follows:

$$\begin{aligned}\dot{\sigma}_h&=e_h\\ \dot{e}_h&=V\sin\gamma\\ \dot{\gamma}&=f_\gamma+g_{\gamma\phi}\phi^c+g_{\gamma\delta}\delta_e^c.\end{aligned} \tag{29}$$

In (29), the added zero dynamics $\dot{\sigma}_h=e_h$ always have an equilibrium $e_h=0$. Therefore, the altitude tracking error e_h can converge to zero as long as (29) is (locally) asymptotically stable, regardless of model uncertainties.

Fixing $\lambda_{c1}=1000$, Fig. 10 shows the root locus of the linearized zero dynamics when λ_{c2} ranges from -1 to 1. It can be seen that there is one real root and two complex roots. The real root goes from right to left as λ_{c2} increases, and lies in LHP when $\lambda_{c2}>0$. The complex roots go from left to right as λ_{c2} increases, and lie in the LHP when $\lambda_{c2}<0.14$. So, the guiding range is $0<\lambda_{c2}<0.14$.

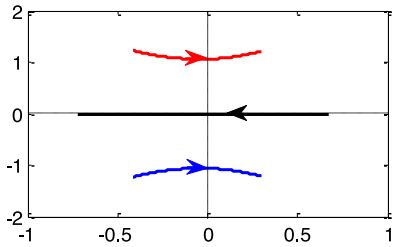

Fig. 10. Root locus of linearized zero dynamics for $\mathbf{y_c}$.

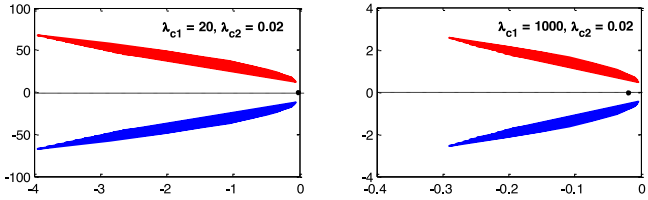

Fig. 11. Root map of linearized zero dynamics for $\mathbf{y_c}$.

Fig. 11 shows the root map of the linearized zero dynamics for all V^*,h^* in Ξ_y with $\lambda_{c1}=20$, $\lambda_{c2}=0.02$ and $\lambda_{c1}=1000$, $\lambda_{c2}=0.02$. It can be observed that all the roots stay in the LHP. So, $\mathbf{y_c}$ is a minimum phase output for these two groups of combination coefficients and can be used for ORDI control. When the new outputs $\mathbf{y_c}=[e_V,e_c]^T$ are driven to zero, then the modified zero dynamics (29) will converge to its equilibrium. Since $e_h=0$ is always an equilibrium of (29), the altitude tracking error e_h will converge to zero even if there are model uncertainties.

2) Controller Design: According to the new external dynamics (26), the control inputs are designed as follows:

$$\begin{bmatrix}\phi\\ \delta_e\end{bmatrix}=\begin{bmatrix}g_V & 0\\ g_{c\phi} & g_{c\delta}\end{bmatrix}^{-1}\begin{bmatrix}-k_{c11}e_V-k_{c12}\sigma_V-f_V\\ -k_{c21}\dot{e}_c-k_{c22}e_c-k_{c23}\sigma_c-f_c\end{bmatrix} \tag{30}$$

where $\dot{\sigma}_c=e_c$, and $k_{c11},k_{c12},k_{c21},k_{c22},k_{c23}$ are positive gains to be designed. Then, the closed-loop system becomes

$$\begin{bmatrix}\dot{e}_V\\ \ddot{e}_c\end{bmatrix}=\begin{bmatrix}-k_{c11}e_V-k_{c12}\sigma_V\\ -k_{c21}\dot{e}_c-k_{c22}e_c-k_{c23}\sigma_c\end{bmatrix}. \tag{31}$$

Finally, the velocity tracking error is determined by the linear equation (31), and the altitude tracking error is determined by the modified zero dynamics (29).

VI. Simulations and Discussions

A. Rigid-Body Model Simulation

To validate the effectiveness of the proposed method, two cases will be considered with Monte Carlo simulations.

Case 1: Nominal model simulation. The proposed methods are applied to the nominal model (1) without uncertainties. The commands are given as $V^*=8000$ ft/s and $h^*=100\,000$ ft.

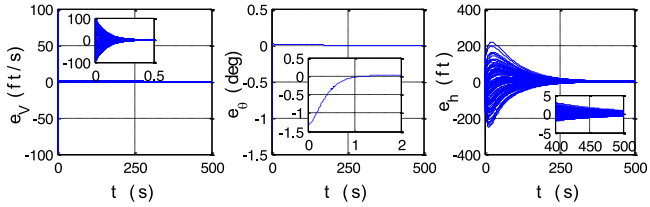

Fig. 12. Nominal model simulation results for $\mathbf{y_a}$.

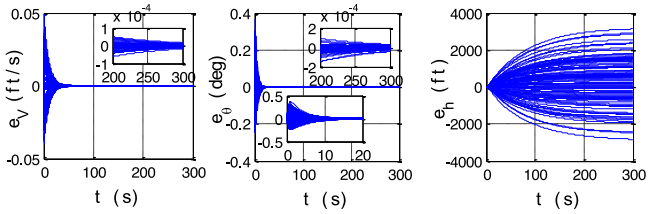

Fig. 13. Uncertain model simulation results for $\mathbf{y_a}$.

The initial values of the outputs are assumed on a random range around the commands: $V(0) = V^* + \Delta_V$ and $h(0) = h^* + \Delta_h$, where $|\Delta_V| \leq 100$ ft/s and $|\Delta_h| \leq 100$ ft.

Case 2: Uncertain model simulation. The proposed methods are applied to the uncertain model. All the aerodynamic parameters in Table II are assumed with uncertainties within 10% of their nominal values. The commands are still given as $V^* = 8000$ ft/s and $h^* = 100\,000$ ft. The initial values of the outputs are set to $V(0) = V^*$ and $h(0) = h^*$.

In both the cases, 100 Monte Carlo simulation runs are taken with the control parameters set as: $k_{a11} = k_{b11} = k_{c11} = k_{a21} = k_{b21} = k_{c21} = 10$, $k_{a12} = k_{b12} = k_{c12} = k_{a23} = k_{b23} = k_{c23} = 1$, $k_{a22} = k_{b22} = k_{c22} = 25$, $\lambda_{c2} = 0.02$.

For $\mathbf{y_a} = [e_V, e_\theta]^T$, in the ideal case without model uncertainties, as shown in Fig. 12, the control outputs e_V, e_θ converge to zero rapidly. Then, e_h converges to a small region around zero slowly under the effect of stable zero dynamics. Therefore, both system outputs almost have no steady-state tracking error.

In the case with model uncertainties, as shown in Fig. 13, the control outputs e_V, e_θ still converge to zero rapidly. Then, e_h becomes stable slowly under the effect of stable zero dynamics, but will not converge to zero. Therefore, velocity has no steady-state error, whereas altitude has large steady-state error.

For $\mathbf{y_b} = [e_V, e_h + \lambda_b e_\theta]^T$, in the ideal case without model uncertainties, the results for $\lambda_b = 20$ and $\lambda_b = 1000$ are shown in Figs. 14 and 15, respectively. As shown in Fig. 14, the control outputs e_V, e_b and e_h, e_θ all converge to nearly zero rapidly. As λ_b increases, the settling time of e_h becomes longer, as shown in Fig. 15. Both system outputs nearly have no steady-state error.

In the case with model uncertainties, it is found that the system is unstable for $\lambda_b = 20$ but is stable for $\lambda_b = 1000$; thus, the robustness is better for larger λ_b. The results for $\lambda_b = 1000$ are shown in Fig. 16. It can be seen that the control outputs e_V, e_b still converge to zero rapidly. Then, e_h, e_θ becomes stable slowly under the effect of stable zero dynamics, but will not converge to zero. So, velocity has no steady-state error, whereas altitude has steady-state error. But the altitude tracking error is much

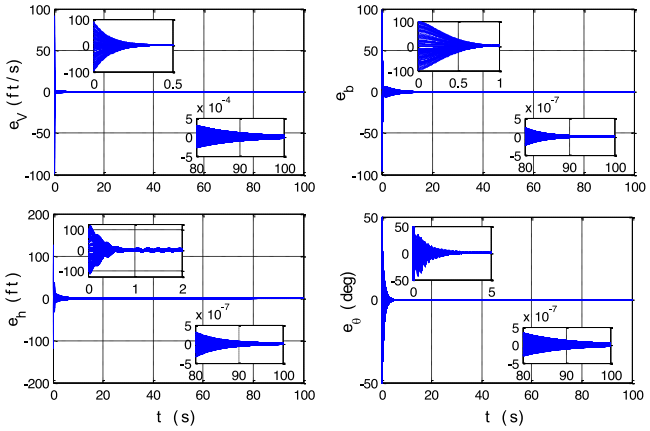

Fig. 14. Nominal model simulation results for $\mathbf{y_b}$ with $\lambda_b = 20$.

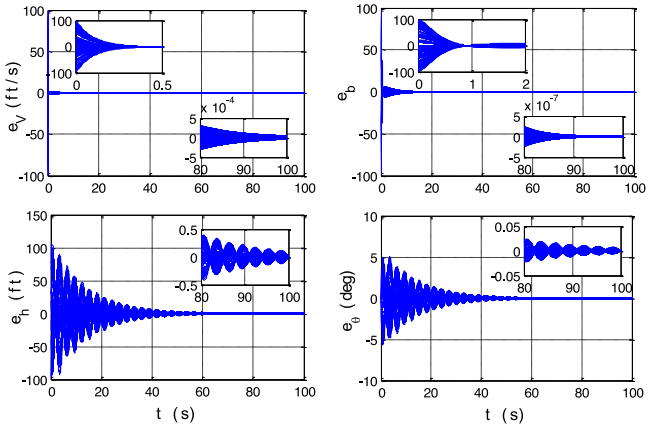

Fig. 15. Nominal model simulation results for $\mathbf{y_b}$ with $\lambda_b = 1000$.

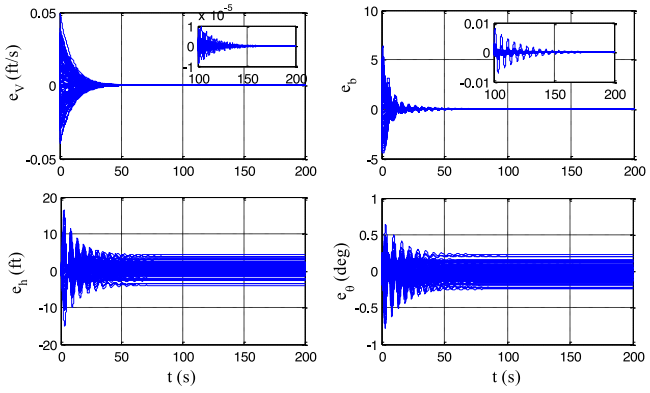

Fig. 16. Uncertain model simulation results for $\mathbf{y_b}$ with $\lambda_b = 1000$.

smaller compared to the results in Fig. 13 when $\mathbf{y_a} = [e_V, e_\theta]^T$ as the output.

For $\mathbf{y_c} = [e_V, e_h + \lambda_{c1} e_\theta + \lambda_{c2} \sigma_h]^T$, in the ideal case without model uncertainties, since $\lambda_{c2} = 0.02$ is very small, the simulation results are very similar to that of $\mathbf{y_b} = [e_V, e_h + \lambda_b e_\theta]$ in the case without model uncertainties. But in the case with model uncertainties, as shown in Fig. 17, the tracking error e_h will still converge to nearly zero due to the integral item in $\mathbf{y_c}$. Finally, both velocity and altitude nearly have no steady-state error.

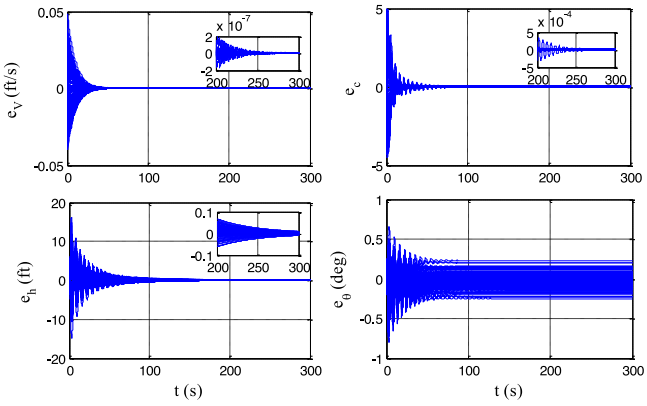

Fig. 17. Uncertain model simulation results for $\mathbf{y_c}$ with $\lambda_{c1} = 1000$.

TABLE III
TRACKING PERFORMANCE INDEX

Control output	Average settling time for nominal model (s)		Average steady-state error for uncertain model (ft/s)	
	e_V	e_h	e_V	e_h
$\boldsymbol{y}_a$	0.29	227.3	3.41×10^{-6}	1067
$\boldsymbol{y}_b\,(\lambda_b = 1000)$	0.29	42.6	1.57×10^{-9}	1.47
$\boldsymbol{y}_c\,(\lambda_{c1} = 1000)$	0.29	51.0	1.55×10^{-8}	3.3×10^{-3}
$\boldsymbol{y}_b\,(\lambda_b = 20)$	0.29	2.92	Unstable	Unstable
$\boldsymbol{y}_c\,(\lambda_{c1} = 20)$	0.29	3.33	Unstable	Unstable

For better comparison of the simulation results, some performance indexes are calculated in Table III, where average settling time is selected as the performance index for the nominal model simulation, and average steady-state error is selected as the performance index for the uncertain model simulation.

From Table III, some interesting observations are found, which are as follows.

1) In this study, velocity remains as a control output but altitude is replaced by a new control output. As shown in Table III, the tracking performance of e_V is generally much better than that of e_h, indicating that the system output being replaced is restricted in tracking performance. This reflects the limitations for these kinds of nonminimum phase systems: only one system output can achieve a prescribed tracking performance.
2) When $\lambda_b = 0$, $\mathbf{y_b} = [e_V, e_h + \lambda_b e_\theta]^T$ is equal to $\mathbf{y} = [e_V, e_h]^T$ and ORDI is equal to standard dynamic inversion, which is unstable for nonminimum phase systems. With $\lambda_b \neq 0$, the zero dynamics can be adjusted. In this sense, ORDI can be seen as a generalization of dynamic inversion control.
3) When $\lambda_b \to \infty$, $\mathbf{y_b} = [e_V, e_h + \lambda_b e_\theta]^T$ is equal to $\mathbf{y_a} = [e_V, e_\theta]^T$. As λ_b increases, the robustness becomes better but the altitude tracking performance becomes worse. Tuning λ_b allows a compromise between robustness and tracking performance.
4) When $\lambda_{c2} = 0$, $\mathbf{y_c} = [e_V, e_h + \lambda_{c1} e_\theta + \lambda_{c2} \sigma_h]^T$ is equal to $\mathbf{y_b} = [e_V, e_h + \lambda_b e_\theta]^T$. By selecting $\lambda_{c2} > 0$, a steady state of zero for both system outputs can be achieved even if there are model uncertainties. But λ_{c2} cannot be too large otherwise it will destroy the stability of the zero dynamics. The effect is very similar to PI control.

TABLE IV
PERFORMANCE UNDER DIFFERENT LEVEL OF UNCERTAINTIES

Level of uncertainties	Average steady-state error of altitude (ft) for $\boldsymbol{y}_b$	Average steady-state error of altitude (ft) for $\boldsymbol{y}_c$
5%	0.75	1.5×10^{-3}
10%	1.47	3.3×10^{-3}
15%	2.04	6.0×10^{-3}
20%	2.82	Unstable

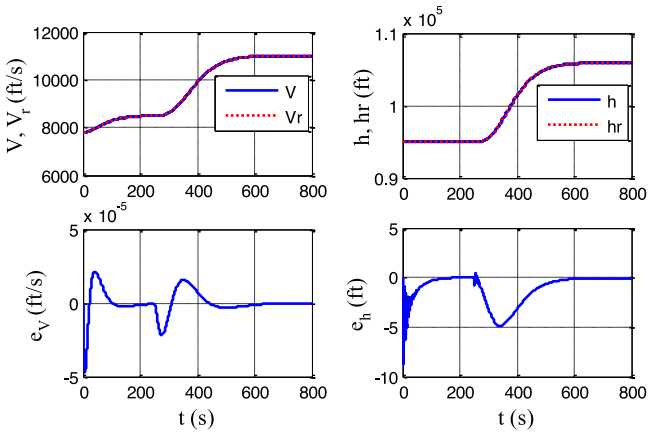

Fig. 18. Maneuver simulation results of ORDI.

Remark 3: The average steady-state errors under different level of uncertainties are shown in Table IV. It can be observed that for the synthetic output with integrator $\mathbf{y_c}$, the steady-state error maintains at almost zero regardless of the uncertainties; whereas for the static synthetic output $\mathbf{y_b}$, the steady-state error is generally small and increases as the uncertainty level grows. However, it should be noted that the integrator in the synthetic output may also make the closed-loop system less robust, as can be seen from the fact that the system with the static synthetic output $\mathbf{y_b}$ can maintain stability under a higher level of uncertainties up to 20%. In practice, if there are no strict requirements of zero steady-state error, static synthetic output would be a good choice.

To make a comparison with other methods applied to a nonminimum phase HSV, an additional maneuver simulation (using the new output y_b with $\lambda_b = 1000$) is made with the same reference commands and initial conditions in [1]. The results are shown in Fig. 18. From the results, it can be seen that both the velocity and the altitude tracking errors converge to small region around zero, and their maximum errors are much smaller than those in [1], which demonstrates the superiority of the developed ORDI method.

Remark 4: In a real-world situation, some other factors such as disturbances, noise, and time delay may also have impact on the control performance. At best, such obstacles result in performance degradation; at worst, they cause instability. Disturbances, unlike parameter uncertainties, are usually time varying, which will make the output deviate from the setpoint. The

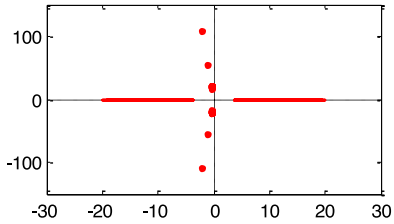

Fig. 19. FHV root map of linearized zero dynamics for $\mathbf{y}$.

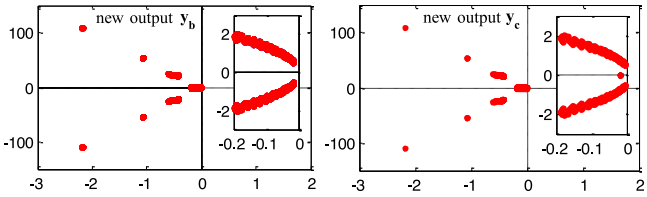

Fig. 20. FHV root map of linearized zero dynamics with output redefinition.

random nature of measurement noise usually causes high-frequency oscillation on the system response. A time delay in the measurement will result in a control action based on obsolete data. For HSV control, it is observed that even a very small level of time delay, say 0.2 s, will cause instability. To mitigate these issues, on one hand, an improved hardware system may be required to reduce measurement noise and time delay; on the other hand, noise filters and disturbance observers can be added to alleviate the influence of noises and disturbances.

B. Flexible Model Simulation

In [23], a more complicated flexible HSV (FHV) model is proposed, which has six flexible states. Since the flexible states are also zero dynamics, it makes the HSV control problem more challenging. Although our control design is based on the rigid-body HSV model, we will show that the controllers developed in this paper are also applicable to FHV.

Using the same method to analyze the FHV zero dynamics, as shown in Fig. 19, it is found that the added six complex roots corresponding to the flexible states are located in the LHP, whereas the other two real roots are the same as those in Fig. 3.

With output redefinition, the zero dynamics are reassigned, as shown in Fig. 20. For the new output $\mathbf{y_b}$, the six complex roots remain in the LHP, whereas the two real roots turn into two LHP complex roots. For the new output $\mathbf{y_c}$, the results are similar except that there is one more real negative eigenvalue. Therefore, stable zero dynamics are obtained for FHV through output redefinition.

To test the tracking performance, using the same reference commands in Fig. 18, the tracking errors are shown in Fig. 21. It can be observed that the tracking errors remain small. Specifically, the velocity tracking error converges to nearly zero in steady state for both $\mathbf{y_b}$ and $\mathbf{y_c}$, whereas the altitude tracking error converges to nearly zero in steady state only for $\mathbf{y_c}$. The amplitude of the flexible states is bounded and become constant in steady state, as shown in Fig. 22.

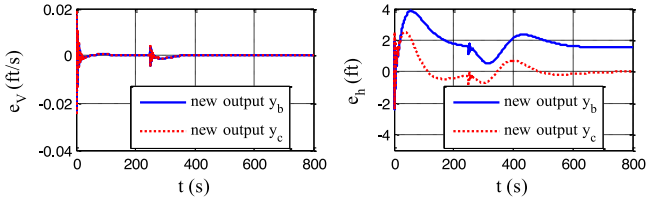

Fig. 21. FHV tracking errors with ORDI control.

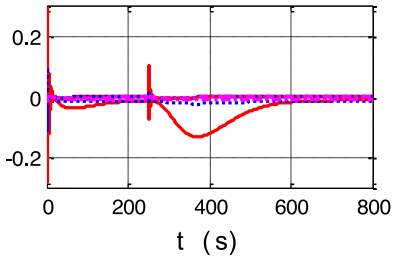

Fig. 22. Amplitude of the flexible states.

VII. Conclusion

An ORDI control scheme is developed for a nonminimum phase HSV. First, the zero dynamics are stabilized by constructing a synthetic output, which is a linear combination of system output, internal variable, and integral tracking error, whose effect is very similar to PI control. Then, the external dynamics are stabilized by dynamic inversion control. It leads to stable zero dynamics while achieving the tracking objective indirectly. Simulation results show that a compromise between robustness and tracking performance can be made by choosing proper values for the combination coefficients. The proposed method is easy to implement and gives much flexibility in the control design. Though aimed at HSVs, the ORDI method has great potential for other systems with unstable zero dynamics. However, in this paper, the new output is a linear combination of system states; thus, the zero dynamics can be only made locally stable. In the future, the new output will be chosen as a nonlinear combination to possibly improve the stability of the zero dynamics.

References

[1] L. Fiorentini and A. Serrani, "Adaptive restricted trajectory tracking for a non-minimum phase hypersonic vehicle model," *Automatica*, vol. 48, no. 7, pp. 1248–1261, 2012.

[2] Q. Zong, J. Wang, and Y. Tao, "Adaptive high-order dynamic sliding mode control for a flexible air-breathing hypersonic vehicle," *Int. J. Robust Nonlinear Control*, vol. 23, no. 15, pp. 1718–1736, 2013.

[3] Q. Zong, J. Wang, B. Tian, and Y. Tao, "Quasi-continuous high-order sliding mode controller and observer design for flexible hypersonic vehicle," *Aerosp. Sci. Technol.*, vol. 27, no. 1, pp. 127–137, 2013.

[4] J. Wang, Q. Zong, R. Su, and B. Tian, "Continuous high order sliding mode controller design for a flexible air-breathing hypersonic vehicle," *ISA Trans.*, vol. 53, no. 3, pp. 690–698, 2014.

[5] Q. Zong, F. Wang, B. Tian, and R. Su, "Robust adaptive dynamic surface control design for a flexible air-breathing hypersonic vehicle with input constraints and uncertainty," *Nonlinear Dyn.*, vol. 78, no. 1, pp. 289–315, 2014.

[6] B. Xu, X. Huang, D. Wang, and F. Sun, "Dynamic surface control of constrained hypersonic flight models with parameter estimation and actuator compensation," *Asian J. Control*, vol. 16, no. 1, pp. 162–174, 2014.

[7] Z. Liu, X. Tan, R. Yuan, G. Fan, and J. Yi, "Immersion and invariance-based output feedback control of air-breathing hypersonic vehicles," *IEEE Trans. Autom. Sci. Eng.*, vol. 13, no. 1, pp. 394–402, Jan. 2016.
[8] O. Ur Rehman, I. R. Petersen, and B. Fidan, "Feedback linearization-based robust nonlinear control design for hypersonic flight vehicles," *Proc. Inst. Mech. Eng., Part I, J. Syst. Control Eng.*, vol. 227, no. 1, pp. 3–11, 2013.
[9] H. An, J. Liu, C. Wang, and L. Wu, "Disturbance observer-based anti-windup control for air-breathing hypersonic vehicles," *IEEE Trans. Ind. Electron.*, vol. 63, no. 5, pp. 3038–3049, May 2016.
[10] M. W. Oppenheimer and D. B. Doman, "Control of an unstable, non-minimum phase hypersonic vehicle model," in *Proc. IEEE Aerosp. Conf.*, pp. 1–7, 2006, doi: 10.1109/AERO.2006.1655985.
[11] X. Hu, C. Hu, L. Wu, and H. Gao, "Output tracking control for nonminimum phase flexible air-breathing hypersonic vehicle models," *J. Aerosp. Eng.*, vol. 28, no. 2, pp.040140631–0401406311, 2013.
[12] J. Parker, A. Serrani, S. Yurkovich, M. Bolender, and D. Doman, "Approximate feedback linearization of an air-breathing hypersonic vehicle," in *Proc. AIAA Guid., Navig., Control Conf. Exh.*, 2006, Paper AIAA 2006–6556.
[13] J. T. Parker, A. Serrani, S. Yurkovich, M. A. Bolender, and D. B. Doman, "Control-oriented modeling of an air-breathing hypersonic vehicle," *J. Guid., Control, Dyn.*, vol. 30, no. 3, pp. 856–869, 2007.
[14] L. Ye, Q. Zong, X. Zhang, and F. Wang, "Control-oriented modeling and adaptive backstepping control for a nonminimum phase hypersonic vehicle," *ISA Trans.*, vol. 70, pp. 161–172, 2017.
[15] A. Serrani, "Nested zero-dynamics redesign for a non-minimum phase longitudinal model of a hypersonic vehicle," in *Proc. IEEE 52nd Annu. Conf. Decis. Control*, 2013, pp. 4833–4838.
[16] S. Devasia, D. Chen, and B. Paden, "Nonlinear inversion-based output tracking," *IEEE Trans. Automat. Control*, vol. 41, no. 7, pp. 930–942, Jul. 1996.
[17] L. Hunt and G. Meyer, "Stable inversion for nonlinear systems," *Automatica*, vol. 33, no. 8, pp. 1549–1554, 1997.
[18] J. Hauser, S. Sastry, and G. Meyer, "Nonlinear control design for slightly non-minimum phase systems: Application to V/STOL aircraft," *Automatica*, vol. 28, no. 4, pp. 665–679, 1992.
[19] S. Gopalswamy and J. K. Hedrick, "Tracking nonlinear non-minimum phase systems using sliding control," *Int. J. Control*, vol. 57, no. 5, pp. 1141–1158, 1993.
[20] M. Fliess, H. Sira-Ramirez, and R. Marquez, "Regulation of non-minimum phase outputs: A flatness based approach," in *Perspectives in Control*. New York, NY, USA: Springer, 1998, pp. 143–163.
[21] M. P. Niemiec and C. Kravaris, "Nonlinear model-state feedback control for nonminimum-phase processes," *Automatica*, vol. 39, no. 7, pp. 1295–1302, 2003.
[22] C. Kravaris, M. Niemiec, and N. Kazantzis, "Singular PDEs and the assignment of zero dynamics in nonlinear systems," *Syst. Control Lett.*, vol. 51, no. 1, pp. 67–77, 2004.
[23] L. Fiorentini, "Nonlinear adaptive controller design for air-breathing hypersonic vehicles," Ohio State Univ., Columbus, OH, USA, 2010.
[24] A. Isidori, *Nonlinear Control Systems*. New York, NY, USA: Springer, 2013.

Linqi Ye received the B.S. degree in automatic control in 2014 from Tianjin University, Tianjin, China, where he has been working toward the Ph.D. degree in control science and engineering in the School of Electrical and Information Engineering since 2014.

He is currently a Visiting Scientist in the Sibley School of Mechanical and Aerospace Engineering, Cornell University, Ithaca, NY, USA. From September 2016 to September 2017, he was a Visiting Scholar in the Department of Mechanical and Aerospace Engineering, The State University of New York at Buffalo.

Qun Zong (M'04) received the B.S., M.S., and Ph.D. degrees in automatic control from Tianjin University, Tianjin, China, in 1983, 1988, and 2002, respectively.

He is currently a Professor in the School of Electrical and Information Engineering, Tianjin University, and the Director of New Aircraft Guidance and Control Center, Ministry of Education in China, Beijing, China. He also serves as an editorial board member of several scientific journals.

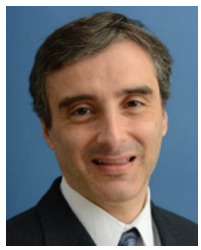

John L. Crassidis received the B.S., M.S., and Ph.D. degrees in mechanical engineering from The State University of New York at Buffalo, Amherst, NY, USA, in 1989, 1991 and 1993, respectively.

He is currently the CUBRC Professor in Space Situational Awareness in the Department of Mechanical and Aerospace Engineering, University at Buffalo, The State University of New York. He was a Postdoctoral Fellow with the NASA Goddard Space Flight Center. He held previous academic appointments at the Catholic University of America and Texas A&M University.

Dr. Crassidis is a Fellow of the American Institute of Aeronautics and Astronautics (AIAA) and the American Astronautical Society. He has received the AIAA Mechanics and Control of Flight Award, the AIAA/ Society of Automotive Engineers (SAE) J. Leland Atwood Award, the SAE Ralph R. Teetor Educational Award, and the AIAA Sustained Service Award.

Bailing Tian (M'11) received the B.S., M.S., and Ph.D. degrees in automatic control from Tianjin University, Tianjin, China, in 2006, 2008, and 2011, respectively.

He is currently an Associate Professor in the School of Electrical and Information Engineering, Tianjin University. From June 2014 to June 2015, he was an Academic Visitor in the School of Electrical and Electronic Engineering, University of Manchester, Manchester, U.K.